Aerodynamic Design and Analysis of a Propeller for a Micro Air Vehicle

Leesang Cho, Jaemin Yoon, Cheolheui Han, Jinsoo Cho*
School of Mechanical Engineering, Hanyang University, Seoul 133-791, Korea

A U-80 propeller and its modified version, U-75 propeller, are used for a micro air vehicle. The performance characteristics of a U-80 propeller and a U-75 propeller have not much known in the published literature. Thus, their aerodynamic characteristics are investigated using a lifting surface numerical method. The lifting surface method is validated by comparing computed results with measured data in a wind tunnel. From the computed results, it is found that the U-75 propeller produces larger thrust with higher efficiency than the U-80 propeller. To enhance the performance of these propellers, a new propeller is designed by following the sequential design procedures with the design parameters such as hub-tip ratio, maximum camber and its position, and chord length distribution along the radial direction. The performance of the designed propeller is shown to be improved much comparing with those of both the U-80 and U-75 propellers.

Key Words : Micro Air Vehicle, "Batwing" MAV, U-80 Propeller, Lifting Surface Method, Micro Air Vehicle Propeller Design

Nomenclature

B : Blade loading
C_P : Power coefficient
C_T : Thrust coefficient
D : Propeller diameter, m
$\vec{i}$: Unit vector
J : Advance ratio
K : Kernel function
$\vec{L}$: Unit vector normal to helical surface
M : Mach number
$\vec{n}$: Unit normal vector
P : Power, watt
P_L : Power loss from induced and viscous drag
Δp : Pressure difference across a lifting surface, Pa
R_{tip} : Propeller tip radius, m
r_{hub} : Propeller hub radius, m
S : Speed ratio
T : Thrust, g_f
t : Time, s
U : Freestream velocity, m/s
$\vec{u}$: Normal velocity, m/s
u, v, w : Velocity components
V_∞ : Flight speed, m/s
v_n : Normal velocity induced on the helical surface, m/s
W : Upwash
x, r, θ : Inertial cylindrical coordinates components
x, y, z : Inertial Cartesian coordinates components
$\bar{x}, r, \bar{\theta}$: Rotational cylindrical coordinates components
$\bar{x}, \bar{y}, \bar{z}$: Rotational Cartesian coordinates components
$\bar{x}_g, \bar{\theta}_g$: Space curve lying on the blade chord surface

Greek Symbols

$\beta_{3/4}$: Blade setting angle, deg.

* Corresponding Author,
E-mail : jscho@hanyang.ac.kr
TEL : +82-2-2220-0429; **FAX** : +82-2-2281-4016
School of Mechanical Engineering, Hanyang University, Seoul 133-791, Korea. (Manuscript **Received** July 4, 2005; **Revised** July 19, 2006)

ε : Control point position
η : Propeller efficiency
ρ : Air density, kg/m^3
ρ_o : Freestream air density, kg/m^3
σ : Helix number
Ω : Blade angular velocity, rad/s
ω : Induced velocity

Subscript

L.E. : Leading edge
T.E. : Trailing edge

Abbreviations

MAV : Micro air vehicle
PABLO: Potential flow around Airfoils with Boundary Layer coupled One-way

1. Introduction

Recently, there have been extensive efforts to develop small-scale aerial vehicles that are as small as possible for special military and civil missions (Muller and DeLaurier, 2001). These unconventional aircraft, called micro air vehicles (MAVs), are flying within the chord-based Reynolds number range from 10^4 to 10^5. The low Reynolds number flight characteristics result in unfavorable aerodynamic characteristic of the low lift-to-drag ratio (Shyy et al., 1999). Therefore a large thrust is inevitable to overcome the low lift-to-drag ratio. The Union U-80 propeller (http://eflightdesigns.com/index.html) is a mainstay in micro-flight vehicle such as the MAV. But, the specification and performance of the U-80 are have not been well known. A "Batwing" MAV (Chung et al., 2004) flies faster than 10 m/s below 14,000 rpm. This flight envelope was hard to accomplish with a commercial U-80 propeller (Hwang et al., 2002). A modified U-80 propeller (U-75 propeller) was applied to the "Batwing" MAV. Both U-80 and U-75 propellers could not produce thrust enough to satisfy the required performance of the "Batwing" MAV. Thus, a new MAV propeller should be designed in order to make a MAV fly faster with long endurance.

Generally, the MAV propeller has been designed using a blade element theory (Mccormick, 1995). The blade element theory determines force and moment by assuming the blade as composition of aerodynamically independent cross-sections, whose characteristics are the same as an airfoil at a proper angle of attack. This theory does not hold for too much loaded propellers; the inception of stall cannot be predicted; the hub and tip losses cannot be evaluated; unsteady and yawed operation are beyond the theory (http://www.aerodyn.org/CFD/VLM/vlm.html). Grasmyer and Keennon (2001) used the minimum induced loss methodology (Adkins and Liebeck, 1983) based on the blade elementary theory to design a MAV propeller. Won et al. (2004) calculated the aerodynamic characteristics of a two-dimensional airfoil using a low speed airfoil analysis code extracted from PABLO (Potential flow around Airfoils with Boundary Layer coupled One-way) (http://www.nada.kth.se/~chris/pablo/pablo.html). Thomson et al. (2004) used Javaprop program (http://www.mh-aerotools.de/airfoils/javaprop.htm) based on the blade element theory to perform the preliminary propeller design. They showed that the blade element theory works well when the power and thrust loadings of the propeller are relatively small. Lee et al. (2002; 2004) applied a blade element theory combined with XFOIL (Drela, 1989) and Betz condition for minimum energy loss (Adkins and Liebeck, 1983) to the low-Reynolds number propeller design.

The nominal performance of a propeller is important to the flight speed and endurance of the developed MAV (Grasmyer and Keennon, 2001). The nominal performance of the propeller can be optimally designed using the inviscid method if we assume that the viscosity has an effect of decreasing performance and this effect is minimum around the nominal design point. Thus, the inviscid method can predict the nominal design point with accuracy in the design step.

In this paper, a lifting surface panel method developed by Williams (1985a; 1985b) for the unsteady aerodynamic and aeroelastic analysis of a single rotation propeller has been applied to predict the performance characteristics of the propeller of all sizes. This method is quite flexible, since it allows the computation of single- and multi-bladed rotors with arbitrary flight path

(http://www.aerodyn.org/CFD/VLM/vlm.html). To validate the present method, computed performance characteristics of the U-75 propeller are compared with the measured data in the wind tunnel.

The U-80 propeller is usually used for the MAV. But, the specification and performance characteristics of the U-80 are has not been well known. In this paper, aerodynamic analysis of the U-80 and the U-75 propellers is carried out to present performance maps for the U-80 and the U-75 propeller users. According to the performance maps, the U-80 and the U-75 propeller can not produce the required thrust for the "Batwing" MAV. Thus, a new MAV propeller is designed in order to make a MAV fly faster with long endurance. With the design requirement of a "Batwing" MAV propeller, a new MAV propeller is designed by evaluating the design parameters on the propeller performance.

2. Lifting Surface Method

The lifting surface method is based on the linearized compressible theory (Heaslet et al., 1950). The propeller blades are assumed to be thin with small local angles of attack. Incident flow distortions involve velocities which are small compared to the helical blade speed. In the linear approximation, the thickness distribution on the airfoil camber the does not affect the loads and will, therefore, be ignored. The basic idea of the lifting surface theory is that the flow field can constructed by superposition of simple harmonic doublets moving along the helical paths swept out by the rotor. The doublet axes are normal to the blade. The task of finding a load distribution is simplified by transferring the boundary conditions from an actual camber surface to a neighboring helical surface. The advantage of this transfer is that the trajectories of all points at a fixed radius on the helical surface are the same (Williams, 1985b).

2.1 Formulation

Consider an initial value problem for linearized compressible flow in which the initial disturbances vanish away from the lifting surfaces. For the load B at a point on a lifting surface $\vec{x}_0$ with unit normal $\vec{n}_0$, a transformed pressure differential $\Delta p = \rho UB$ is assigned acting in the direction $+\vec{n}_0$ (We will assume that $\vec{n}_0$ has no component in the freestream or x direction. The flow has speed U, density ρ, and Mach number M). The lifting surface induces a transformed velocity at an arbitrary point $\vec{x}$, in an arbitrary direction $\vec{n}$, which is given by an integral over the lifting surface.

$$w(\vec{x}) = \iint K(\vec{x}, \vec{x}_0)\, B(\vec{x}_0)\, dS \tag{1}$$

The kernel is the fundamental solution of the reduced wave equation corresponding to the velocity w induced at $\vec{x}$ by a point load applied at $\vec{x}_0$. In the standard problem, w is specified on the surface and we solve for the load B.

In this paper, the frequency domain lifting surface method and rigid wake model for the MAV propeller were used. Rigid wake is modeling along the helical surface generated due to propeller rotation. Wake effect on the MAV propeller was considered using the kernel function.

2.2 Linearized compressible flow theory

The continuity and momentum equations can be obtained by application of the divergence theorem. The continuity equation is shown as

$$\frac{\partial \rho}{\partial t} + \nabla \cdot (\rho \vec{V}) = 0 \tag{2}$$

and the momentum equation, neglecting gravitational effects, is shown as

$$\rho \frac{D\vec{V}}{Dt} = -\nabla p \tag{3}$$

The continuity and the momentum equations for irrotational flows ($\nabla \times \vec{V} = 0$) are given by

$$\begin{aligned} &\left(1-\frac{u^2}{a^2}\right)\frac{\partial u}{\partial x} + \left(1-\frac{v^2}{a^2}\right)\frac{\partial v}{\partial y} + \left(1-\frac{w^2}{a^2}\right)\frac{\partial w}{\partial z} \\ &-2\frac{uv}{a^2}\frac{\partial u}{\partial y} - 2\frac{vw}{a^2}\frac{\partial v}{dz} - 2\frac{uw}{a^2}\frac{\partial w}{\partial x} \\ &+\frac{1}{\rho}\frac{\partial \rho}{\partial t} - \frac{u}{a^2}\frac{\partial u}{\partial t} - \frac{v}{a^2}\frac{\partial v}{\partial t} - \frac{w}{a^2}\frac{\partial w}{\partial x} = 0 \end{aligned} \tag{4}$$

More detailed explanation is introduced in the reference (Cho and Williams, 1993).

2.3 Coordinates and geometry

Figure 1 shows propeller coordinates system to analyze the propeller performance. Coordinate system is composed of inertial and rotor frames. The flow condition and boundary condition are converted into the rotor frame.

In inertial frame, (x, y, z) is a right handed Cartesian coordinate system fixed in the undisturbed fluid. And, (x, r, θ) are cylindrical coordinate system, with θ measured from the z-axis.

$$y=r\sin\theta,\ z=r\cos\theta \tag{5}$$

In this frame the propeller center of rotation advances with speed U along the $(-x)$ axis, and the blade rotate clockwise at speed Ω when viewed from the $(-x)$ axis (so the rotational velocity vector is located on the $(+x)$ axis).

In rotor frame, $(\bar{x},\ \bar{y},\ \bar{z})$ is a right handed Cartesian coordinate system fixed in rotor. And, $(\bar{x}, r, \bar{\theta})$ are cylindrical coordinate system fixed in the rotor.

2.4 Helical surface

Figure 2 shows helical surface generation to find a load distribution by transferring the boundary conditions from an actual camber surface to a neighboring helical surface.

Any fixed point on a blade follows a helical trajectory.

$$x-\frac{U}{\Omega}\theta=\bar{x}-\frac{U}{\Omega}\bar{\theta} \tag{6}$$

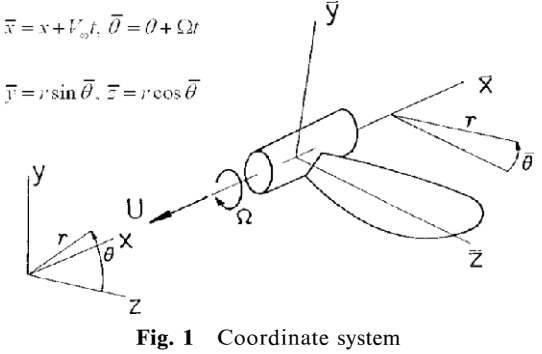

Fig. 1 Coordinate system

Let $\bar{x}_g(r)$, $\bar{\theta}_g(r)$ define some space curve lying on the blade chord surface. This curve generates a helical surface as follows.

$$x=\frac{U}{\Omega}(\theta+\sigma),\ \sigma(r)\equiv\frac{\Omega}{U}\bar{x}_g-\bar{\theta}_g \tag{1}$$

This helical surface is time-independent, and is fixed by the advance ratio and the choice of generator curve (which determines $\sigma(r)$).

The unit normal vector to the helical surface, $\vec{L}$, can be expressed in Eq. (9). Note that the normal vector $\vec{L}$ is a function of position only.

$$\vec{L}=\nabla\left(x-\frac{U}{\Omega}(\theta+\sigma)=\vec{i}-\frac{U}{\Omega r}(\vec{i}_\theta-a\vec{i}_r)\right)$$
$$a=r\frac{d\sigma}{dr} \tag{8}$$

where $(\vec{i},\ \vec{i}_\theta,\ \vec{i}_r)$ are unit vectors in the (x, θ, r) directions respectively.

In the aerodynamic model, the load distribution is placed on the helical surface.

$$r_h<r<r_t$$
$$\bar{\theta}_{L.E}(r)<\bar{\theta}<\bar{\theta}_{T.E}(r) \tag{9}$$

These edge coordinates of the lifting surface are obtained by projecting the blade chordline onto the helical surface.

$$\bar{\theta}_{T.E}-\bar{\theta}_{L.E}=\left|\frac{(\Delta x)^2+(r\Delta\theta)^2}{(U/\Omega)^2+r^2}\right|^{1/2} \tag{10}$$

2.5 Surface boundary condition

The normal velocity component of the fluid velocity on the blade surface must be equal to the

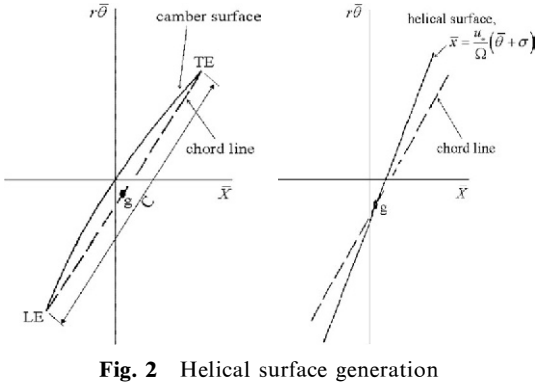

Fig. 2 Helical surface generation

normal velocity component of the blade surface.

$$\vec{n}\cdot\vec{u}=v_n \tag{11}$$

In the present study the normal velocity is assumed to be either steady or simple harmonic at any fixed blade point. For steady state operation, the normal velocity can be expressed in Eq. (12).

$$v_n=-Un_n-\Omega(\bar{z}n_y-\bar{y}n_z) \tag{12}$$

2.6 Lifting surface integral equation

From the assumptions of aerodynamic linearity, simple harmonic time dependence, and blade to blade periodicity, the entire disturbance field surrounding the propeller can be determined directly from the distribution of load amplitude over the reference blade. In particular, then, the load distribution determines the distribution of normal velocity over the reference blade.

This relationship between load and normal velocity can be expressed as an integral equation.

$$W(\bar{r},\bar{\theta})=\int_{\bar{r}_h}^{1}\int_{\bar{\theta}_{LE}}^{\bar{\theta}_{TE}}B(\bar{r}_0,\bar{\theta}_0)\frac{\partial}{\partial\bar{\theta}}K(\bar{\theta}-\bar{\theta}_0,\bar{r},\bar{r}_0)\,\bar{r}_0 d\bar{\theta}_0 d\bar{r}_0 \tag{13}$$

where

$$W=4\pi\left(\frac{\vec{L}\cdot\vec{u}}{U}\right)e^{i\bar{\omega}\bar{\theta}},\quad B=S^2\left(\frac{\Delta p}{\rho_0 U^2}\right)e^{i\bar{\omega}\bar{\theta}_0} \tag{14}$$

Here, W is proportional to the normal velocity, B is proportional to the pressure jump across the blade, and K is a (known) kernel function. In most applications the normal velocity is specified and the integral equation can be solved for the load distribution.

2.7 Discretization of the integral equation

As shown in Fig. 3, the blade camber surface is discretized with small rectangular elements. The normal velocity W is specified at one point per element, thereby reducing the integral equation to a set of simultaneous algebraic equations for the loads on each element.

After discretizing the blade surface with several elements, we can specify the lifting surface integral equation assuming the pressure on the element surface is constant. The lifting surface integral equation, (13), admits an infinite number of solutions.

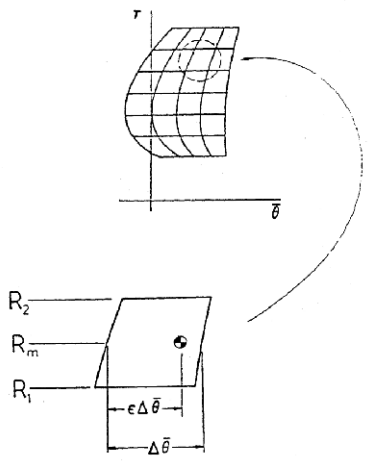

Fig. 3 Discretization of a propeller surface and control point placement

However, only one is physically acceptable — the one which satisfies the Kutta condition, $\Delta p=0$ at trailing edge.

A control point is placed on the mean radius of each panel with $\bar{\theta}$ and distance $\varepsilon\Delta\bar{\theta}$ downstream from the midspan panel leading edge, where $\Delta\bar{\theta}$ is the panel chord at midspan (Fig. 3). The algebraic system can be obtained from this discretization ($W_i=W$ at i-th control point $(\bar{\theta}_i,\bar{r}_i)$ and $B_j=B$ on J-th panel).

$$\begin{aligned} W_i&=\sum_{j=1}^{NP}C_{ij}B_j \\ C_{ij}&=\iint\frac{\partial K(\bar{\theta}_i-\bar{\theta}_0,\ \bar{r}_i\bar{r}_0)}{\partial\bar{\theta}_0}d\bar{\theta}_0\bar{r}_0 d\bar{r}_0 \end{aligned} \tag{15}$$

2.8 Propeller performance

The thrust and power of a propeller are normally expressed in coefficient form. The performance variables of the present study are defined as follows.

Advance Ratio,

$$J=\frac{\pi V_\infty}{R_{tip}\Omega}$$

Thrust Coefficient,

$$C_T=\frac{\pi^2 T}{4\rho\Omega^2 R_{tip}{}^4} \tag{16}$$

Power Coefficient,

$$C_P=\frac{\pi^2 P}{4\rho\Omega^3 R_{tip}{}^5}$$

Efficiency,

$$\eta=J\frac{C_T}{C_P}$$

Here V_∞ is a flight speed, Ω is an angular velocity, and R_{tip} is a blade tip radius.

The efficiency of the propeller is the ratio of the work done in forward motion to that in rotational motion,

$$\eta=\frac{U\cdot T}{U\cdot T+P_L} \tag{17}$$

where P_L is the power loss from induced and viscous drag.

Neglecting viscous losses, P_L is the rate of work done by the pressure forces acting over the blade,

$$P_L=-\iint p\vec{n}\cdot\vec{u}\,dA \tag{18}$$

3. Results and Discussion

3.1 Aerodynamic analysis of U-80 and U-75 propellers

Figure 4 shows the blade geometries of the U-80 and U-75 propellers. The three-dimensional geometry for the Union U-80 propeller was obtained using a measuring instrument. Blade pitch angle, camber and maximum thickness for the Union U-80 propeller were measured at each section along the radial direction. In this figure, the U-75 propeller is obtained from cutting the U-80's blade tip by an amount of 2.5 mm.

Figure 5 shows the performance characteristics of the U-80 propeller. The peak efficiency is 70.47% at J=0.5. This peak efficiency at a low advance ratio means that it should be used at a relatively slow flight speed for a given rotational speed.

In Fig. 6, the performance map of the U-80 propeller is plotted for the change of the rotational speed and the flight speed. The region A represents the region which the propeller efficiency is more than 70%. The propeller efficiency is less than 60% in the region B. The required

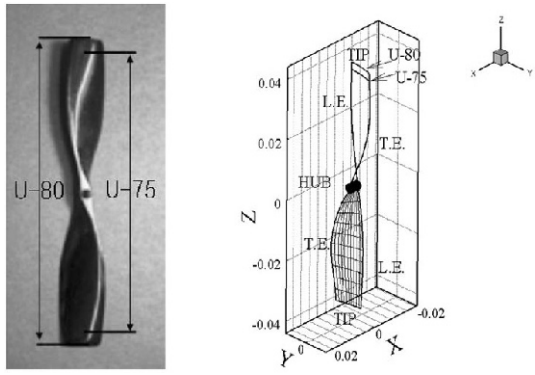

(a) Blade geometries of U-80 and U- 75 propellers

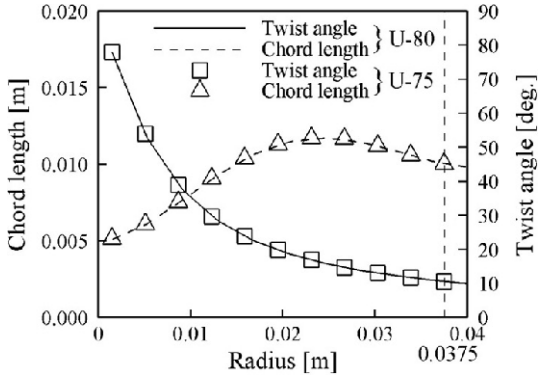

(b) Chord length and twist angle distributions

Fig. 4 Geometry of U-80 and U-75 propellers

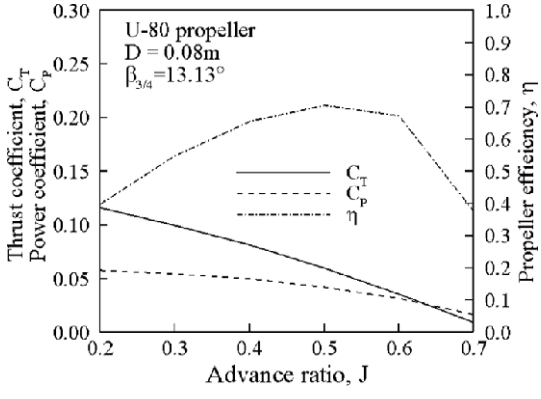

Fig. 5 Characteristic curve of a U-80 propeller

thrust for the "Batwing" MAV is 0.182 N. The current version of the "Batwing" MAV requires the thrust of at least 20 gf. From the present computed results, it can be concluded that, to obtain a thrust of 20 gf, the U-80 propeller should operate at more than 14,000 rpm with the flight speed

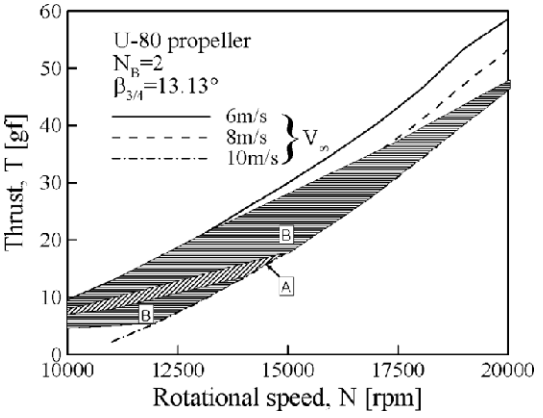

Fig. 6 Performance map of U-80 propeller (B : region that has the efficiency of more than 60%, A : region that has the efficiency of more than 70%)

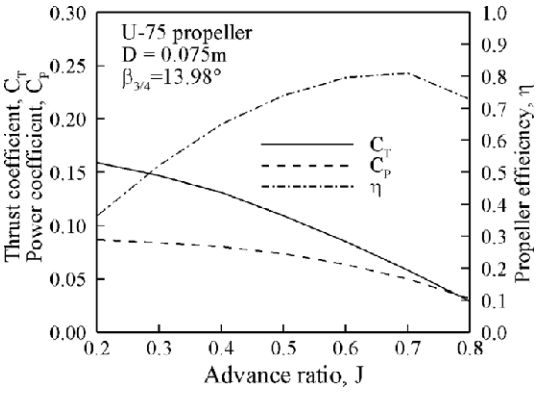

Fig. 7 Characteristic curve of U-75 propeller

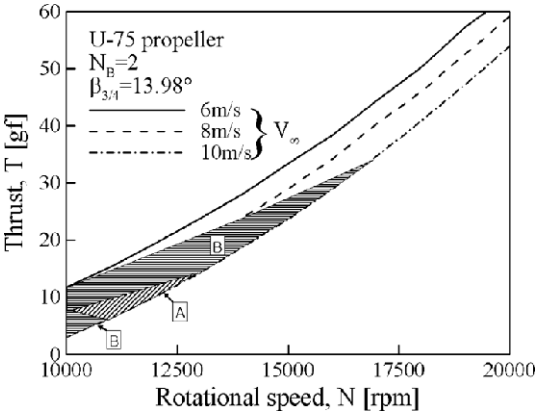

Fig. 8 Performance map of U-75 propeller (B : region that has the efficiency of more than 70%, A : region that has the efficiency of more than 80%)

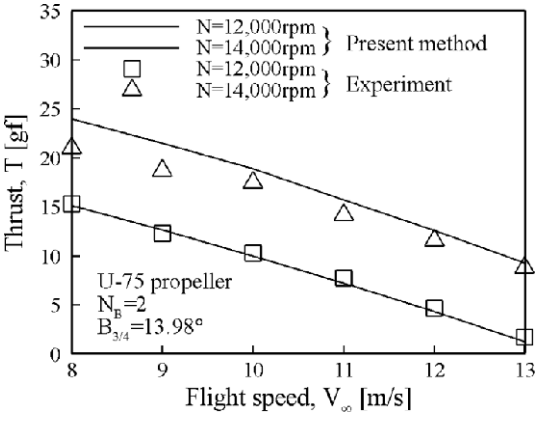

Fig. 9 Comparison with experimental results of U-75 propeller

of 6 m/s under the efficiency of less than 57.99%.

Figure 7 shows the characteristic curve of the U-75 propeller. In the figure, the U-75 propeller has a peak efficiency of 81.16% at J=0.7. This peak efficiency at a larger advance ratio means that the U-75 propeller can be applied to a high-speed flight.

Figure 8 shows the performance map of U-75 propeller. It can be deduced from the figure that the MAV with the U-75 propeller can fly at 9 m/s with the thrust of 20 gf at 14,000 rpm and with an efficiency of more than 75.11%. The U-75 propeller has the increase in the flight speed by 3m/s and in the efficiency by 17% compared with the U-80.

In Fig. 9, present method is validated by comparing the computed results with the measured data in the wind tunnel (Hwang et al., 2002). In the figure, the viscous effect is shown to be dominant under the flight speed of less than 10 m/s. The present method does not consider the viscous effect in predicting the performance of the propeller. However, present results agree well with the measured data when the flight speed is more than 10 m/s.

3.2 Aerodynamic Design of a Propeller for a "Batwing" MAV

The design requirements of the "Batwing" are

provided by a "Batwing" team at Konkuk University (Hwang et al., 2002). These design requirements are as follows : the rotational speed of 13,000 rpm, the flight speed of 14 m/s, the thrust of more than 20 gf, and the peak efficiency of more than 80%.

The design of a propeller for the "Batwing" MAV is done following the design procedure in Fig. 10. The effect of the hub-tip ratio on the propeller's performance is investigated for r/R_{tip}= 0.04, 0.06, and 0.08, respectively. An ideal twist angle distribution is selected as a reference twist angle distribution, and then the design twist angle distribution is specified by checking the computed performance data.

The maximum camber, the position of the maximum camber, and the chord length distribution are also selected in order to satisfy the design requirements. When the performance of the designed propeller does not satisfy the design requirements at each design step, the design process is started again at the previous design step.

The hub-tip ratios of both the U-80 and U-75 propellers are 0.04. The effect of the hub-tip ratio on the propeller's performance is investigated by changing the hub-tip ratio from 0.04 to 0.08.

As shown in Fig. 11, the hub-tip ratio does not affect the propeller's performance much. The aerodynamic efficiency of the MH-75 propeller is peak at the hub-tip ratio of 0.06. So, we selected the hub-tip ratio of 0.06 to design a MH-75 propeller.

In Fig. 12, the effect of the twist angle distribution is plotted. Near the hub, the for the variation of twist angle distribution ideal twist angle distribution has larger values than the designed twist angle distribution. The computed results for an ideally-twisted propeller show negative sectional

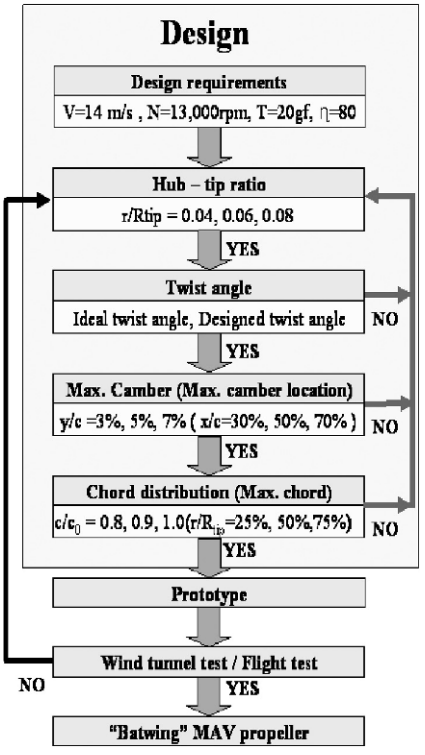

Fig. 10 Design procedure for a "Batwing" MAV propeller

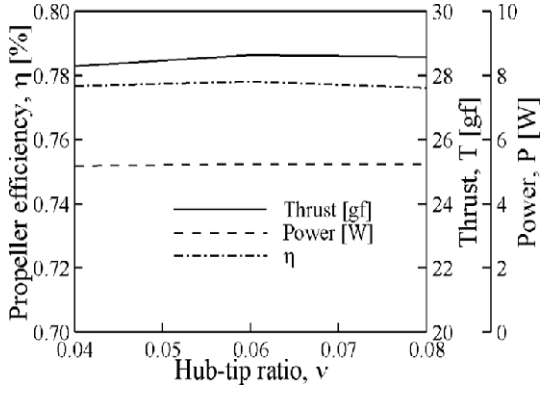

Fig. 11 Performance curves for the variation of hub-tip ratio

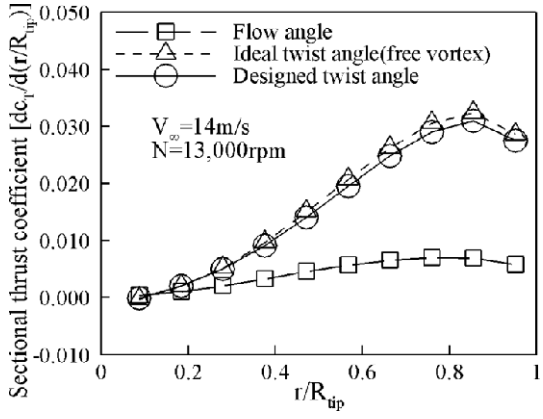

Fig. 12 Sectional thrust coefficient distributions for the variation of twist angle distribution

thrust coefficients that will decrease the total thrust.

The flow in an annular passage of the propeller has no radial velocity component which is axisymmetric, is commonly known as radial equilibrium flow. Free vortex flow means that the product of radius and tangential velocity is constant ($rc_\theta = const.$). The twist angle distribution of the MAV propeller is designed using the free vortex flow with radial equilibrium flow assumption. As shown in Fig. 13, the twist angle near the hub is modified in order to make twist angles near the hub higher than flow angles and to have smooth twist angle distributions.

In Fig. 14, propeller with ideal twist angle distribution has high total thrust at the same operating condition. On the other hand, aerodynamic efficiency is decreased because the input power is increased due to reverse thrust in the hub region. Therefore, twist angle of the MH-75 propeller is redesigned with decrement of the blade pitch angle at the hub.

The NACA 4-digit series is used for the airfoil of the "Batwing" propeller. To investigate the effect of the maximum camber on the propeller's performance, the maximum cambers are selected as 3%, 5%, and 7% of the chord length (Fig. 15 (a)). The effect of the position of the maximum camber is investigated by setting it as 30%, 50% and 70% of the chord length from the leading edge of the airfoil, respectively (See Fig. 15(b)). As the maximum camber increases and the position of maximum camber moves toward the trailing edge, the thrust increases with the efficiency stepping down.

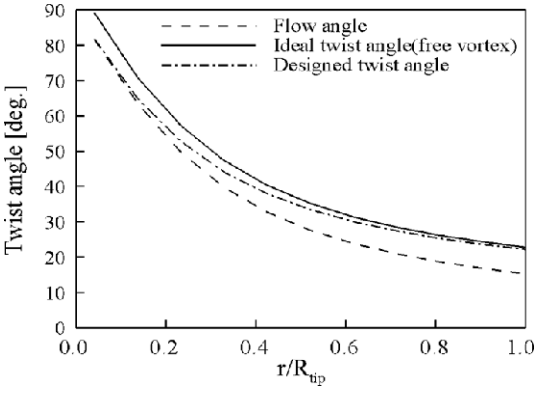

Fig. 13 Flow angle and twist angle distributions of "Batwing" propeller

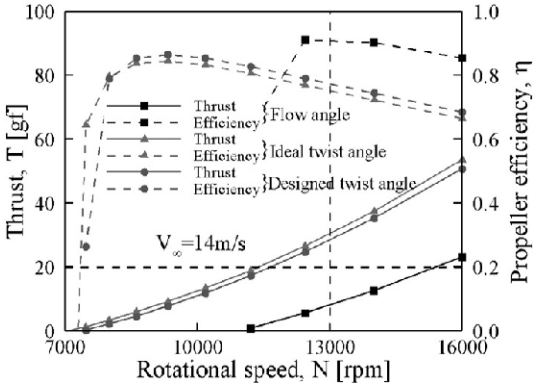

Fig. 14 Performance curves according to the variation of the twist angle distributions

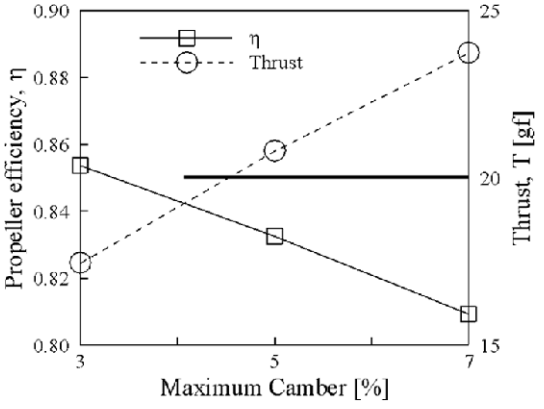

(a) Maximum camber

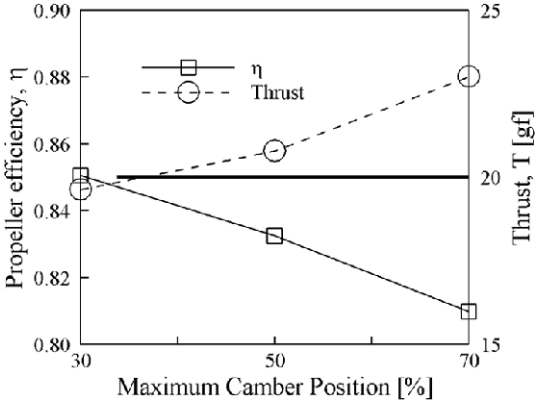

(b) Maximum camber position

Fig. 15 Maximum camber and its position

In spite of the variation of the distance from the leading edge to the location of the maximum camber, "BATWING" MAV propeller can not produce larger thrust than 20 gf at the maximum camber of 3% of the chord. In case of 5% maximum camber and 50% maximum camber location, the highest efficiency is obtained. A NACA 5500 airfoil section is selected as an optimized airfoil shape for the newly designed propeller.

In Fig. 16(a), the effect of the position of the maximum chord length on the performance is plotted. The investigated three cases of the position of the maximum chord length are 25%, 50% and 75% of the span, respectively. When the position of the maximum chord length is located at the 75% span, the thrust is more than 20 gf.

The effect of the maximum chord length on the performance is studied for four cases of the maximum chord length (case 1 ; 6.88 mm, case 2 ; 7.74 mm, case 3 ; 8.6 mm and case 4 ; 9.46 mm). When the maximum chord length increases, the thrust increases with the efficiency stepping down. As shown in Fig. 16(b), the designed propeller of case 2 produces a thrust of more than 20 gf with a high efficiency of around 84 percent.

Figure 17 shows the blade geometry of a "Batwing" propeller designed by following above sequential design procedures. Fig. 17 shows the geometrical shape, the chord length and twist angle distributions of the "Batwing" propeller. The diameter of the "Batwing" MAV propeller is 75 mm. The airfoil section is NACA 5505. Fig. 17(b) shows the chord length and twist angle distributions of both the U-75 and the "Batwing" propeller. The U-75 propeller has the maximum chord length at the 60% of the span while the "Batwing"

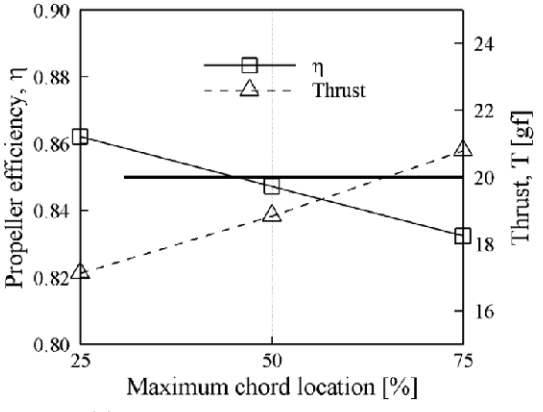

(a) Maximum chord length position

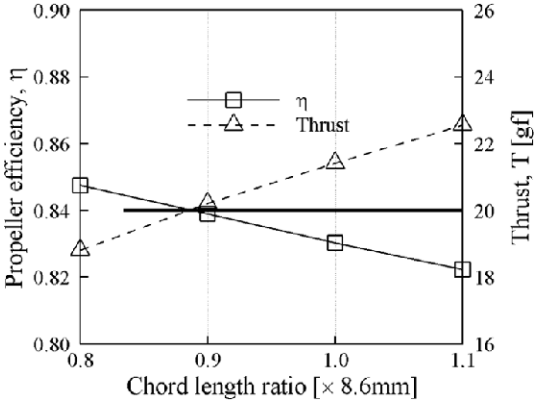

(b) Maximum chord length

Fig. 16 Maximum chord and its position

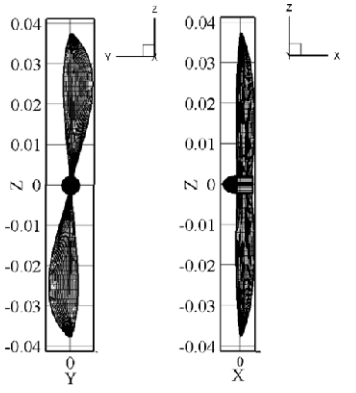

(a) Front and side view

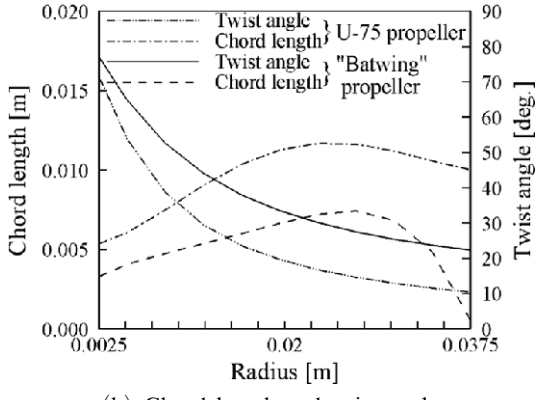

(b) Chord length and twist angle

Fig. 17 Blade geometries of the designed "Batwing" MAV propeller

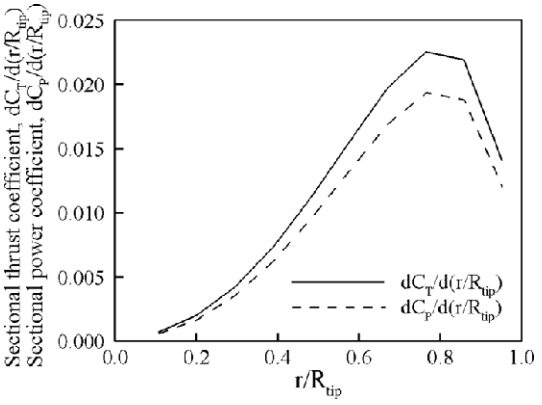

Fig. 18 Sectional thrust and power coefficient distribution of the "Batwing" MAV propeller

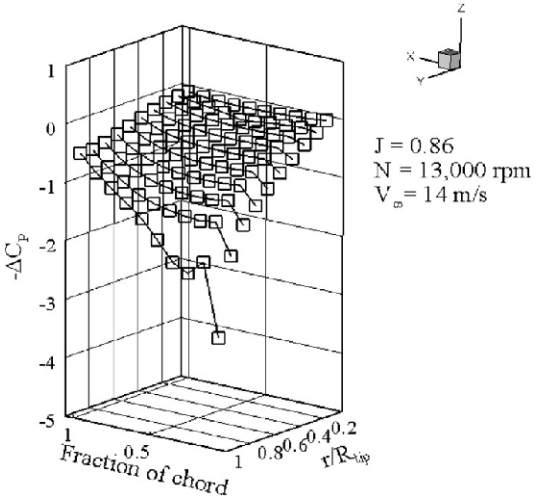

Fig. 19 Sectional pressure distribution of the designed "Batwing" MAV propeller

propeller has the maximum chord length at the 75% span.

Figure 18 shows the sectional thrust and power coefficient distributions of the "Batwing" MAV propeller. The positions of maximum sectional thrust and power coefficient are about $r/R_{tip}=$ 0.8. Sectional thrust and power coefficients are decreased near the blade tip region due to the tip losses.

Figure 19 shows the pressure distributions on the "Batwing" MAV propeller. The pressure distribution is uniform along the spanwise direction except the blade tip region where pressure difference is decreased by the tip leakage flow.

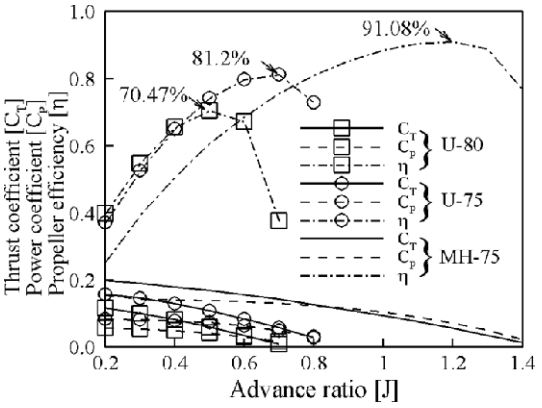

Fig. 20 Characteristic curves of the designed "Batwing" MAV propeller compare with U-80 and U-75 propellers

Figure 20 shows the characteristic curves of the U-80, U-75, and "Batwing" MAV propellers. The peak efficiency of the "Batwing" MAV propeller is 91.08% at J=1.2 which is higher than those of the U-80 and U-75 propellers. It can be deduced from the results that the present design methodology is working for the MAV propeller design.

5. Conclusions

The present study on the performance characteristics of both the U-80 and U-75 propellers shows that the U-80 propeller has both low flight speed and low efficiency. The U-75 propeller, modified version of the U-80 propeller, has better performance than the U-80 propeller. However, the U-75 propeller is not satisfactory for the "Batwing" MAV.

A sequential design procedure is completed by investigating the effect of following parameters on the performance of the MAV propeller. The hub-tip ratio shows no effect on the performance of the propeller. The ideal twist angle distribution produces negative sectional thrust distribution near the hub. The twist angle near the hub is modified in order to increase the sectional thrust. Design parameters such as the maximum camber, the maximum chord length, the position of maximum camber toward the airfoils' trailing edge have the effect of increasing the thrust with effi-

ciency stepping down. The peak efficiency of the designed "Batwing" MAV propeller is higher than the U-80 and U-75 propellers at the higher flight speed.

In the present method, the effect of low Reynolds number flow is ignored. Hence, the next work will include the effect of low Reynolds number flow.

Acknowledgements

This work was supported by Grant No.(R01-2005-000-10310-0) from the Basic Research Program of the Korean Science and Engineering Foundation.

References

Adkins, C. N. and Liebeck, R. H., 1983, "Design of Optimum Propellers," AIAA Paper 84-0190.

Cho, J. S. and Williams, M. H., 1993, "S-plane Aerodynamics of Nonplanar Lifting surfaces," *Journal of Aircraft*, Vol. 30, No. 4, pp. 433～438.

Chung, D. K., Hwang, H. K., Kim, J. H., Park, H. C. and Yoon, K. J., 2004, "Development of Micro Air Vehicle System "BATWING" with Fixed Wing," *Journal of The Korean Society for Aeronautical and Space Sciences*, Vol. 32, No. 2, pp. 82～87.

Drela, M., 1989, "XFOIL : An Analysis and Design for Low Reynolds Number Airfoil," *Low Reynolds Number Aerodynamics*, Springer-Verlag, New York, pp. 1～12.

Grasmyer, J. M. and Keennon, M. T., 2001, "Development of the Black Widow Micro Air Vehicle," AIAA paper 2001-0127.

Heaslet, M. A., Lomax, H. and Spreiter, J. R., 1950, "Linearized Compressible-Flow Theory for Sonic Flight Speeds," NACA Report 956 NACA-TN-1824.

Hwang, H. K., Kim, J. H., Chung, D. K., Yoon, K. J., Lee, Y. J. and Kang T. S., 2002, "Development of Micro Air Vehicle "SPOT"," The 8th Symposium on Aircraft Development Technology, May 2002.

Karz, J. and Plotkin, A., 1991, *Low speed aerodynamics from Wing Theory to Panel Method*, McGraw-Hill, Inc.

Lee, K. H., Jeon, Y. H., Bae E. S., Lee, D. H. and Lee, K. T., 2004, "Implementation of the Numerical Optimization for the Micro-Air Vehicle Propeller," 10th AIAA/ISSMO Multidisciplinary Analysis and Optimization Conference (AIAA 2004-4428).

Lee, K. H., Kim, K. H., Bae E. S., Lee, K. T. and Ahn, J., 2002, "Design and Analysis for the Propeller of MAVs in Low Reynolds Number Flows," *KSAS*, Vol. 30, No. 5, pp. 1～8.

Mccormick, B. W., 1995, *Aerodynamics, Aeronautics and Flight Mechanics*, 2nd Edition, John Wiley & Sons, Inc.

Muller, T. J. and DeLaurier, J. D., 2001, "An Overview of Micro Air Vehicle Aerodynamics," *Fixed and Flapping Wing Aerodynamics for Micro Air Vehicle Applications*, Edited by Muller, T. J., *Progress In Astronautics and Aeronautics*, Vol. 195, AIAA, Inc., 1801 Alexander Bell Drive, Reston, Virginia 20191-4344.

Shyy, W., Berg, M. and Ljungqvist, D., 1999, "Flapping and Flexible Wings for Biological and Micro Air Vehicle," *Progress in Aerospace Sciences*, Vol. 35, pp. 455～505.

Thompson, P., Ward, G., Kelman, B. and Null, W., 2004, "Design Report : Development of Surveillance, Endurance, and Ornithoptic Micro Air Vehicles," 8th International Micro Air Vehicle Competition conference.

Williams, M. H., 1985a, "An Unsteady Lifting Surface Theory for Single Rotation Propellers," Purdue University Report.

Williams, M. H., 1985b, "User Guide to UPROP3S," Purdue University Report.

Won, H. T., Nam, T. W., Lim, D. W. and Collins, K. B., 2004, "Georgia Institute of Technology Micro Air Vehicle Design Team Report for the 2004 MAV Competition," 8th International Micro Air Vehicle Competition conference.

http ://eflightdesigns.com/index.html

http ://www.aerodyn.org/CFD/VLM/vlm.html

http ://www.nada.kth.se/ ～chris/pablo/pablo.html

http://www.mh-aerotools.de/airfoils/javaprop.htm